Citation: Claessens S.J. and C. Hirt (2013) Ellipsoidal topographic potential – new solutions for spectral forward gravity modelling of topography with respect to a reference ellipsoid, Journal of Geophysical Research (JGR) – Solid Earth, 118(11), 5991-6002, doi: 10.1002/2013JB010457.

Ellipsoidal topographic potential – new solutions for spectral forward gravity modelling of topography with respect to a reference ellipsoid

S.J. Claessens

Western Australian Centre for Geodesy & The Institute for Geoscience Research,

Curtin University, GPO Box U1987, Perth, WA 6845, Australia

Email: s.claessens@curtin.edu.au

C. Hirt

Western Australian Centre for Geodesy & The Institute for Geoscience Research,

Curtin University, GPO Box U1987, Perth, WA 6845, Australia

Email: c.hirt@curtin.edu.au

Abstract

Forward gravity modelling in the spectral domain traditionally relies on spherical approximation. However, this level of approximation is insufficient for some present-day high accuracy applications. Here we present two solutions that avoid the traditional spherical approximation in spectral forward gravity modelling. The first solution (the extended integration method) applies integration over masses from a reference sphere to the topography, and applies a correction for the masses between ellipsoid and sphere. The second solution (the harmonic combination method) computes topographic potential coefficients from a combination of surface spherical harmonic coefficients of topographic heights above the ellipsoid, based on a relation among spherical harmonic functions introduced by Claessens (2005, *J. Geod.* 79, 398-406). Using a degree-2160 spherical harmonic model of the topographic masses, both methods are applied to derive Earth's ellipsoidal topographic potential in spherical harmonics. The harmonic combination method converges fastest, and – akin to the EGM2008 geopotential model – generates additional spherical harmonic coefficients in spectral band 2161 to 2190 which are found crucial for accurate evaluation of the ellipsoidal topographic potential at high degrees. Therefore, we recommend use of the harmonic combination method to model ellipticity in spectral-domain forward modelling. The method yields ellipsoidal topographic potential coefficients which are 'compatible' with global Earth geopotential models constructed in ellipsoidal approximation, such as EGM2008. It shows

that the spherical approximation significantly underestimates degree correlation coefficients among geopotential and topographic potential. The topographic potential model is, for example, of immediate value for the calculation of Bouguer gravity anomalies in fully ellipsoidal approximation.

1 Introduction

Modelling of the gravitational potential generated by the topography of the Earth and other celestial objects has long been an active field of research. Knowledge of the topographic potential is useful mainly because the short-wavelength signal of observed gravity-related quantities is strongly dominated by the contribution from the topography. It can therefore be used to predict a detailed gravity field where no or only few observations are available. This is important for the construction of high-resolution Earth gravity models [e.g., *Pavlis and Rapp* 1990, *Pavlis et al.* 2012], modelling of the gravity field of celestial objects such as the Moon, Mars and Venus [e.g., *Wieczorek* 2007, *Hirt et al.* 2012a], and the creation of synthetic Earth gravity models [e.g., *Haagmans* 2000, *Claessens* 2003, *Bagherbandi and Sjöberg* 2012].

A second major range of applications uses the differences between a model of the topographic potential and the contribution of topography from observed gravity-related quantities. Most importantly, this gives insight into mass irregularities within the planet's interior [e.g., *Völgyesi and Toth* 1992, *Wieczorek and Phillips* 1998]. The resulting signal is much smoother than the actual gravity field, which also facilitates data prediction and downward continuation of satellite observations [e.g. *Heck and Wild* 2005, *Grombein et al.* 2013]. A related subject is that of terrain corrections in geoid determination according to Stokes's theory, which requires the removal of all masses outside the geoid [e.g., *Sjöberg* 1998, *Sun* 2002].

Generation of a topographic potential model requires forward modelling of mass contributions through Newton's integral, either in the space domain or in the spectral domain. Topography can be either uncompensated [e.g., *Hirt et al.* 2012b], or an isostatic compensation can be assumed [e.g., *Rummel et al.* 1988, *Grafarend and Engels* 1993]. See *Tsoulis* [2001] and *Göttl and Rummel* [2009] for a further discussion on isostatic compensation mechanisms and the topographic-isostatic potential.

Many different methods for forward modelling in the space domain have been developed; an overview of and comparisons between the different methods are provided in *Heck and Seitz* [2007] and *Tenzer et al.* [2010]. Comparisons of forward modelling in the space and spectral domain are provided by *Kuhn and Seitz* [2005], *Wild-Pfeiffer and Heck* [2007] and *Balmino et al.* [2012].

Forward modelling in the spectral domain is computationally more efficient and has been widely used for several decades. The resolution of topographic potential models have increased from spherical harmonic degree and order 180 in the 1980s [*Rapp* 1982, *Rummel et al*. 1988] to 10,800 recently [*Balmino et al.* 2012]. The increase in resolution demands more precise modelling methodologies.

A common technique employed in spectral forward modelling is the use of a series expansion of powers of the topographic height and surface spherical harmonic coefficients (SHCs) of these powers of topographic height to generate solid SHCs of the topographic potential. Early contributions have used a linear approximation [e.g, *Lambeck* 1979, *Rapp* 1982]. *Rummel et al.* [1988] extended this to third-order powers and *Balmino et al.* [1994] generalised it to higher-order powers. Convergence of the series expansion was studied by *Sun and Sjöberg* [2001], *Novák* [2010] and *Hirt and Kuhn* [2012].

One subject that has received little attention thus far is the evaluation of errors introduced by the spherical approximation that is used almost universally. In spectral forward modelling, a mass-sphere is used as a reference, and the planet's topography is assumed to reside on this spherical surface. It is well-known that the Earth is to a much higher degree of accuracy modelled by an oblate ellipsoid of revolution. This is commonly accounted for in the creation of global gravity models [e.g., *Pavlis et al.* 2012], but not in spectral forward modelling, which makes topographic potential models incompatible with global gravity models. The topographic potential generated taking into account the planet's ellipticity is herein called the ellipsoidal topographic potential (ETP).

Sjöberg [2004] derives ellipsoidal corrections to topographic effects in geoid modelling, but this work does not provide a methodology for generating the ETP. Furthermore, the corrections derived were limited to the order of the squared first numerical eccentricity of the ellipsoid e^2, which is insufficient for high degree and order SHCs. To our knowledge, spectral forward modelling of the ETP has been studied only by *Novák and Grafarend* [2005], *Balmino et al.* [2012] and *Wang and Yang* [2013].

Novák and Grafarend [2005] model the ETP and its vertical gradient by a series of base functions that are orthonormal on the ellipsoid [*Grafarend and Engels* 1992], using geodetic coordinates. These base functions are different from the spherical harmonic functions used in global gravity models, so the resulting expansion of the ETP is not directly compatible with global gravity models. The approach has also not been applied globally, and the convergence of the series expansions has not been studied. *Balmino et al.* [2012] provide a method to compute the ETP using surface spherical harmonic expansions, but they use the spherical approximation for their numerical computations (up to d/o 10,800). They did compute ellipsoidal corrections, but only for long wavelengths (up to d/o 120). *Wang and Yang* [2013] use two methods to compute the ETP: a spherical harmonic solution that requires a global integration for every degree n, and a solution using ellipsoidal harmonics which is implemented up to degree and order 180 only.

In this paper, two methods that avoid the classical spherical approximation in spectral domain forward-modelling are introduced. Both methods use surface spherical harmonic expansions with respect to a reference ellipsoid. Use of only spherical harmonics has several advantages over ellipsoidal harmonics: it is simple, does not require the use of ellipsoidal coordinates, and the resulting expansion of the ETP is directly compatible with global gravity models. It also avoids numerical issues in the computation of ellipsoidal harmonic functions [e.g., *Sona* 1995], although much improvement in this field has been made recently [e.g., *Sebera et al.* 2012, *Fukushima* 2013].

The first of our two methods is similar to one suggested by *Balmino et al.* [2012]; it is also similar to the spherical harmonic solution by *Wang and Yang* [2013], but it uses binomial expansions instead of 'brute-force' computations that include a global integration for every degree n. The second method is a new, different method which will prove to have significant advantages.

The two methods are derived in section 2. In section 3 they are compared to the spherical approximation and to one another, both theoretically and numerically, and the resulting power spectrum of the ETP is compared to that of the EGM2008 global gravity model [*Pavlis et al.* 2012]. Some examples of applications are provided in section 4, and the final section contains a discussion of the results.

2 Methods

2.1 Topographic potential

The spherical harmonic expansion of the gravitational potential of a body is [e.g., *Rummel et al.* 1988]

$$V(P) = \frac{GM}{R}\sum_{n,m}\left(\frac{R}{r_P}\right)^{n+1} \bar{V}_{nm}^{R}\,\bar{Y}_{nm}\,(P) \tag{1}$$

where $V(P)$ is the gravitational potential in point P, G is the universal gravitational constant, M is the mass of the body, R is a reference sphere radius, r_P is the distance between point P and the coordinate system origin, n, m are the spherical harmonic degree and order, $\bar{Y}_{nm}$ are fully normalised (4π-normalised) spherical harmonic functions, and the SHCs $\bar{V}_{nm}^{R}$ are [*Rummel et al.* 1988]

$$\bar{V}_{nm}^{R} = \frac{1}{M(2n+1)}\int_{\Sigma}\left(\frac{r_Q}{R}\right)^{n} \rho_{\Sigma}(Q)\,\bar{Y}_{nm}\,(Q)d\Sigma_Q \tag{2}$$

where the integration is over the whole body (domain Σ) and $\rho_{\Sigma}(Q)$ is the density of the body in evaluation point Q. In spherical coordinates, Eq. (2) reads

$$\bar{V}_{nm}^{R} = \frac{1}{M(2n+1)}\int_{\theta=0}^{\pi}\int_{\lambda=0}^{2\pi}\int_{r=0}^{r_{\Sigma}(\theta,\lambda)}\left(\frac{r_Q}{R}\right)^{n} \rho_{\Sigma}(Q)\,\bar{Y}_{nm}\,(Q) r_Q^2 \sin\theta\, d\theta d\lambda dr \tag{3}$$

where θ is the spherical polar co-latitude, λ is the longitude, r is the distance from the origin and $r_{\Sigma}(\theta, \lambda)$ is the distance between the origin and the body surface.

The topographic potential is commonly defined as the potential generated by topographic masses, either with respect to the geoid [e.g., *Sjöberg* 1998] or the reference ellipsoid [e.g., *Novák and Grafarend* 2005, *Vajda et al.* 2007]. A further alternative, less common in geodesy, is to define the topography with respect to a spherical surface, using topographic heights above a sphere [e.g., *Wieczorek and Phillips* 1998]. *Balmino et al.* [2012] discuss the differences between these definitions. Here, we use a definition with respect to the ellipsoid.

We define the topographic potential as the difference between potentials generated by a) a body with irregular topography and density distribution $\rho_{\Sigma}(Q)$ (Eq. 3) and b) a reference ellipsoid with density distribution $\rho_e(Q)$, where $\rho_e(Q) = \rho_{\Sigma}(Q)$ for all points Q that fall inside both the body (Σ) and the ellipsoid. As a result, it contains the combined effect of topographic masses above the ellipsoid (where terrain height is positive) and the lack of topographic mass under the ellipsoid (where terrain height is negative).

The SHCs of the topographic potential are then

$$\bar{V}_{nm}^{R} = \frac{R^2}{M(2n+1)} \int_{\theta=0}^{\pi} \int_{\lambda=0}^{2\pi} V^T(\theta,\lambda)\, \bar{Y}_{nm}(\theta,\lambda) \sin\theta \, d\theta d\lambda \tag{4}$$

where

$$V^T(\theta,\lambda) = \begin{cases} \displaystyle\int_{r=r_e}^{r_\Sigma} \left(\frac{r_Q}{R}\right)^{n+2} \rho_\Sigma(Q)\, dr \quad \text{for} \quad r_\Sigma > r_e \\ \displaystyle -\int_{r=r_\Sigma}^{r_e} \left(\frac{r_Q}{R}\right)^{n+2} \rho_e(Q)\, dr \quad \text{for} \quad r_\Sigma < r_e \end{cases} \tag{5}$$

and r_e is the distance from the origin to an ellipsoidal reference surface (the ellipsoidal radius). Note that the square of the reference radius has been moved outside the integrals in Eq. (4) for mathematical convenience. To allow analytical integration over r in Eq. (5), the density is usually assumed radially invariant. An alternative that assumes a variable density function as a power series of the radial distance is provided in *Ramillien* [2002]. In the case of radial invariance, the integral in Eq. (5) is simple, and identical for both cases

$$V^T(\theta,\lambda) = \frac{R\rho(\theta,\lambda)}{n+3}\left[\left(\frac{r_\Sigma}{R}\right)^{n+3} - \left(\frac{r_e}{R}\right)^{n+3}\right] \tag{6}$$

where $\rho(\theta,\lambda) = \rho_\Sigma$ for $r_\Sigma > r_e$ and $\rho(\theta,\lambda) = \rho_e$ for $r_\Sigma < r_e$.

Where information about radial variations in density within the topography is available, the topography can be replaced by a layer of constant density and the same mass as the original layer: the equivalent rock topography/rock-equivalent topography (ERT/RET) [e.g., *Balmino et al.* 1973, *Tsoulis* 1999, *Hirt et al.* 2012b]. The height of this layer, the rock-equivalent height, can be computed in planar approximation [e.g., *Balmino et al.* 1973, *Rummel et al.* 1988, *Hirt et al.* 2012b] or in spherical approximation [e.g., *Claessens* 2003, *Mladek* 2006]. It is customary to replace ocean water, fresh lake water and ice by equivalent rock layers, resulting in negative RET heights over all of Earth's oceans [e.g., *Hirt et al.* 2012b].

Lateral variations in density can be accommodated by using surface density functions [*Kuhn and Featherstone* 2003], by using different surface harmonic analyses over various domains [*Balmino et al.* 2012], or by including the density function in the global integration within the spherical harmonic analyses [*Eshagh* 2009, *Tenzer et al.* 2012]. In the remainder of this paper, we assume constant density of rock-equivalent topography $(\rho(\theta,\lambda) = \rho)$ for the sake of simplicity, but our results can be extended to accommodate laterally variant density using one of the above-mentioned methods. An isostatic compensation mechanism can also be applied to generate the so-called topographic-isostatic potential [e.g. *Rapp* 1982, *Sünkel* 1986, *Rummel et al.* 1988]. Here, we only consider the uncompensated topographic potential, but our results can easily be extended to also include an isostatic compensation part.

2.2 Ellipsoidal topographic potential

In practical applications of spectral forward modelling of the topographic potential, a spherical approximation is commonly applied to simplify Eq. (6). The approximations made are

$$r_e = R \tag{7}$$

and

$$r_\Sigma = R + H \tag{8}$$

where H is the orthometric height of the topography. However, this spherical approximation is no longer sufficient, especially for spectral analysis of high-degree and -order SHCs.

Instead of the spherical approximations in Eqs. (7) and (8), we use Eq. (6) in unaltered form. The spherical harmonic synthesis in Eq. (4), with Eq. (6), could be performed numerically [*Wang and Yang* 2013], but this is computationally inefficient because V^T is dependent on spherical harmonic degree n. To make the computations more efficient, a binomial expansion can be applied to the terms in Eq. (6) that are dependent on n. This is commonly done in spherical approximation [e.g., *Rummel et al.* 1988, *Wieczorek and Phillips* 1998], and can also be applied in the current ellipsoidal approximation. In spherical approximation, the second term between the square brackets in Eq. (6) cancels, but it needs to be taken into account in ellipsoidal approximation. Below, we derive two different methods to do this.

2.3 Method 1: Extended integration (EI) method

The first term within the square brackets in Eq. (6) can be expanded into a binomial series [cf. *Claessens* 2006]

$$\left(\frac{r_\Sigma}{R}\right)^{n+3} = \sum_{k=0}^{n+3} \binom{n+3}{k} \left(\frac{l_\Sigma}{R}\right)^k = 1 + \sum_{k=1}^{n+3} \frac{1}{k!} \prod_{j=1}^{k} (n+4-j) \left(\frac{l_\Sigma}{r_e}\right)^k \tag{9}$$

where

$$l_\Sigma = r_\Sigma - R \tag{10}$$

Note that the reference radius of the spherical harmonic expansion R is commonly set equal to the semi-major axis of the geodetic reference ellipsoid. Given the Earth's flattening, l_Σ reaches values with an absolute magnitude in excess of 20 km near the poles on Earth.

A similar binomial series can be applied to the second term within the square brackets in Eq. (6)

$$\left(\frac{r_e}{R}\right)^{n+3} = \sum_{k=0}^{n+3} \binom{n+3}{k} \left(\frac{l_e}{R}\right)^k \tag{11}$$

where

$$l_e = r_e - R \tag{12}$$

Inserting Eqs. (9) and (11) into Eq. (6) gives

$$V^T(Q) = \frac{R\rho}{n+3} \sum_{k=1}^{n+3} \binom{n+3}{k} \left[\left(\frac{l_\Sigma}{R}\right)^k - \left(\frac{l_e}{R}\right)^k \right] \tag{13}$$

The summation runs from $k = 1$, because the term with $k = 0$ vanishes. Inserting Eq. (13) into Eq. (4) and rearranging the order of summation and integration gives

$$\bar{V}_{nm}^R = \frac{\rho R^3}{M(2n+1)(n+3)} \sum_{k=0}^{n+3} \binom{n+3}{k} \left[\int_\sigma \left(\frac{l_\Sigma}{R}\right)^k \bar{Y}_{nm}(Q) d\sigma - \int_\sigma \left(\frac{l_e}{R}\right)^k \bar{Y}_{nm}(Q)\, d\sigma \right] \tag{14}$$

The two integrations over the unit sphere can be combined into one, but we separate them here, as it provides a useful interpretation of the process when compared to the spherical approximation. Equation (14) can be simplified to

$$\bar{V}_{nm}^R = \frac{4\pi\rho R^3}{M(2n+1)(n+3)} \left[\sum_{k=1}^{n+3} \binom{n+3}{k} \left(\bar{l}_{nm}^{(k)} - \overline{le}_{nm}^{(k)} \right) \right] \tag{15}$$

where we have introduced the following fully normalised surface spherical harmonic series

$$\left(\frac{l_\Sigma}{R}\right)^k = \sum_{n,m} \bar{l}_{nm}^{(k)} \bar{Y}_{nm} \tag{16}$$

with

$$\bar{l}_{nm}^{(k)} = \frac{1}{4\pi} \int_\sigma \left(\frac{l_\Sigma}{R}\right)^k \bar{Y}_{nm}\, d\,\sigma \tag{17}$$

and

$$\left(\frac{l_e}{R}\right)^k = \sum_{n,m} \overline{le}_{nm}^{(k)} \bar{Y}_{nm} \tag{18}$$

with

$$\overline{le}_{nm}^{(k)} = \frac{1}{4\pi} \int_\sigma \left(\frac{l_e}{R}\right)^k \bar{Y}_{nm}\, d\,\sigma \tag{19}$$

This shows that it is possible to model the topographic potential with respect to the ellipsoid using only spherical harmonics.

Comparing Eq. (15) to the solutions in spherical approximation of *Rummel et al.* [1988] and *Wieczorek and Phillips* [1998], it is obvious that this method essentially computes the contribution from the sphere to the topography (taken with respect to the ellipsoid, resulting in integration over a generally extended range) and then subtracts the contribution from the mass between the sphere and the ellipsoid. *Balmino et al.* [2012] have derived a solution similar to this, but appear not to have implemented it.

Because the series in Eq. (15) converges, not all $n+3$ terms need to be taken into account but the series can be truncated after sufficient precision has been obtained. If applied to Earth, series convergence is slower than in spherical approximation, because l_Σ and l_e reach significantly larger magnitudes than the rock-equivalent heights. The rate of convergence is shown in section 3.2.

2.4 Method 2: Harmonic combination (HC) method

A second, new method avoids the use of l_Σ and l_e, which are large over much of the Earth's surface. It is based on a different binomial expansion of the second term in Eq. (6), taking into account that the ellipsoidal surface is easily described mathematically as a function of latitude [e.g., *Claessens* 2006]. It also relies on a relation among spherical harmonic functions derived by *Claessens* [2005].

First, Eq. (6) is rewritten as follows

$$V^T(Q) = \frac{R\rho}{n+3}\left(\frac{r_e}{R}\right)^{n+3}\left[\left(\frac{r_\Sigma}{r_e}\right)^{n+3} - 1\right] \tag{20}$$

We now apply a binomial series expansion to the term between square brackets

$$\left(\frac{r_\Sigma}{r_e}\right)^{n+3} - 1 = \sum_{k=1}^{n+3}\binom{n+3}{k}\left(\frac{d_\Sigma}{r_e}\right)^k = \sum_{k=1}^{n+3}\frac{1}{k!}\prod_{j=1}^{k}(n+4-j)\left(\frac{d_\Sigma}{r_e}\right)^k \tag{21}$$

where

$$d_\Sigma = r_\Sigma - r_e \tag{22}$$

The distance d_Σ closely approximates the ellipsoidal height of the rock-equivalent topography, but is measured along the direction to the ellipsoid's origin. Inserting Eqs. (20) and (21) into Eq. (4) gives, after changing the order of integration and summation

$$\bar{V}_{nm}^R = \frac{R^2}{M(2n+1)}\frac{R\rho}{n+3}\sum_{k=1}^{n+3}\binom{n+3}{k}\int_\sigma \left(\frac{r_e}{R}\right)^{n+3}\left(\frac{d_\Sigma}{r_e}\right)^k \bar{Y}_{nm}(Q)d\sigma \tag{23}$$

We now apply a second binomial series to the first term within the integral [cf. *Claessens* 2006]

$$\left(\frac{r_e}{R}\right)^{n+3} = \left(\frac{b}{R}\right)^{n+3} (1 - e^2 \sin^2\theta)^{-\frac{n+3}{2}}$$
$$= \left(\frac{b}{R}\right)^{n+3} \sum_{j=0}^{\infty} (-1)^j \binom{-\frac{n+3}{2}}{j} e^{2j} \sin^{2j}\theta \tag{24}$$

As is common in geodesy, we have here assumed that the reference ellipsoid is an oblate ellipsoid of revolution defined by its semi-major axis a and semi-minor axis b or squared first numerical eccentricity e^2. Note the difference with the binomials series used in method 1 (Eq. 11). The series in Eq. (24) is infinite, but *Claessens* [2006] has shown that it always converges. Convergence is most rapid for low degrees n. We also apply the following relation among spherical harmonic functions of equal order m [*Claessens* 2005, Eq. 27]

$$\sin^{2j}\theta\, \bar{Y}_{nm} = \sum_{i=-j}^{j} \bar{K}_{nm}^{2i,2j} \bar{Y}_{n+2i,m} \tag{25}$$

where $\bar{K}_{nm}^{2i,2j}$ are fully normalised sinusoidal Legendre weight functions [*Claessens* 2005, 2006], which can be computed through the recursion relations in Appendix A. Inserting Eqs. (24) and (25) into Eq. (23) gives

$$\bar{V}_{nm}^{R} = \frac{R^2}{M(2n+1)} \frac{R\rho}{n+3} \left(\frac{b}{R}\right)^{n+3}$$
$$\times \sum_{k=1}^{n+3} \binom{n+3}{k} \sum_{j=0}^{\infty} (-1)^j \binom{-\frac{n+3}{2}}{j} e^{2j} \sum_{i=-j}^{j} \bar{K}_{nm}^{2i,2j} \int_{\sigma} \left(\frac{d_\Sigma}{r_e}\right)^k \bar{Y}_{n+2i,m}(Q)\, d\sigma \tag{26}$$

Introducing the following fully normalised surface spherical harmonic series

$$\left(\frac{d_\Sigma}{r_e}\right)^k = \sum_{n,m} \bar{d}_{nm}^{(k)} \bar{Y}_{nm} \tag{27}$$

where

$$\bar{d}_{nm}^{(k)} = \frac{1}{4\pi} \int_{\sigma} \left(\frac{d_\Sigma}{r_e}\right)^k \bar{Y}_{nm}\, d\sigma \tag{28}$$

gives the final expression for the solid SHCs of the ETP

$$\bar{V}_{nm}^{R} = \frac{4\pi\rho b^3}{M(2n+1)(n+3)} \left(\frac{b}{R}\right)^{n} \sum_{k=1}^{n+3} \binom{n+3}{k} \sum_{j=0}^{\infty} (-1)^j \binom{-\frac{n+3}{2}}{j} e^{2j} \sum_{i=-j}^{j} \bar{K}_{nm}^{2i,2j}\, \bar{d}_{n+2i,m}^{(k)} \tag{29}$$

This method thus relies on a combination of surface SHCs of equal order m. The summations over k and j can be truncated; the rate of convergence is shown in section 3.3. When a spherical reference surface is selected, the solutions of both methods (Eqs. 15 and 29) degenerate into the well-known spherical approximation [e.g., *Rummel et al.* 1988, *Wieczorek and Phillips* 1998]

$$\bar{V}_{nm}^{R} = \frac{4\pi\rho R^3}{M(2n+1)(n+3)} \sum_{k=1}^{n+3} \binom{n+3}{k} \bar{H}_{nm}^{(k)} \tag{30}$$

where

$$\bar{H}_{nm}^{(k)} = \frac{1}{4\pi} \int_{\sigma} \left(\frac{H}{R}\right)^k \bar{Y}_{nm}\, d\,\sigma \tag{31}$$

Balmino et al. [2012] derive an ellipsoidal correction to the spherical approximation which, like our solution, involves a summation over surface SHCs of equal order m. However, their corrections use an expansion of the ellipsoidal radius to the first order of the ellipsoid's flattening. This is akin to truncating Eq. (24) after $j = 1$, which is insufficient for high degree SHCs due to the appearance of degree n in the binomial coefficient.

3 Numerical study

3.1 General remarks

The primary purpose of the numerical study is to (i) analyse the convergence behaviour of the EI-method and the HC-method (cf. Sect. 2.3 and 2.4) separately, and (ii) compare the methods to gain insight into similarities and differences. In all tests, we use the RET2012 rock-equivalent topography model developed at Curtin University. RET2012 is a spherical-harmonic model of Earth's uncompensated topographic masses complete to degree and order 2160, which corresponds to 5 arc-min spatial resolution. It describes the masses of (i) Earth's visible topography, (ii) ocean water, (iii) major ice-sheets of Greenland and Antarctica, and (iv) major inland lakes (of North America and Asia) using a single constant mass-density of 2670 kg m^{-3} . The compression of water and ice masses was accomplished as described in *Hirt et al.* [2012b, Sect 3.2] for a degree-360 predecessor of the degree-2160 RET2012 model. Full details on data sets and methods used is in *Hirt* [2013, Appendix A]. The SHCs of RET2012 are publicly available via http://geodesy.curtin.edu.au/research/models/Earth2012/, file Earth2012.RET2012.SHCto2160.dat.

Our numerical tests use the geometrical and physical parameters of the GRS80 reference ellipsoid: semi-major axis a = 6378137 m, semi-minor axis b = 6356752.3141 m, and GM = 3.986005 × 10^{14} m^3 s^{-2} [*Moritz* 2000]. With the CODATA (Committee on Data for Science and Technology) numerical value for G = 6.67384 × 10^{-11} m^3 kg^{-1} s^{-2} [*Mohr et al.* 2012, p 72], it follows for Earth's mass: M = 5.9725810 × 10^{24} kg. For all spherical approximations tested in this study, we use the GRS80 semi-major axis a as the reference sphere radius R.

Testing of the two methods described in Sect. 2 requires geocentric radii of the topography r_Σ which were obtained from expanding the RET2012 topography to degree and order 2160. The quantities l_Σ (Eq. 10), l_e (Eq. 12) and d_Σ (Eq. 22) and the topographic height functions (THF) l_Σ/R , l_e/R and d_Σ/r_e were prepared in terms of 2 arc-min global grids (however, due to the limited resolution of the RET2012 model these grids do not contain information at spatial scales smaller than 5 arc-min) . The THFs were then raised to integer powers k (ranging from 1 up to 25) and the resulting $(l_\Sigma/R)^k$, $(l_e/R)^k$ and $(d_\Sigma/r_e)^k$ harmonically analysed to give sets of SHCs $\bar{l}_{nm}^{(k)}$, $\overline{le}_{nm}^{(k)}$ and $\bar{d}_{nm}^{(k)}$. Note that surface spherical harmonic expansions are not restricted to data being on a sphere [e.g., Jekeli 1988]. All spherical harmonic analyses were carried out to degree and order 2699 with the algorithm of *Driscoll and Healy* [1994] as implemented in the SHTools package (http://shtools.ipgp.fr/). Note that the resulting expansions lack power in the highest degrees due to the limited resolution of the RET2012 model. However, these expansions were only used to degree 2160 (EI-method) and 2220 (HC-method).

3.2 Method 1: Extended integration (EI) method

We investigated the convergence of the ellipsoidal topographic potential from the EI-method by evaluating Eq. (18) separately for integer powers of the THF from $k = 1$, $k = 2$ to $k = 25$. The (dimensionless) potential degree variances of the resulting contributions $\bar{V}_{nm}^{R\,(k)}$ are shown in Fig. 1 together with the total (accumulative) $\bar{V}_{nm}^{R}$ resulting from addition of the first 25 contributions.

From Fig. 1, integer contributions are required up to $k = 22$ to sufficiently converge at degree and order 2160. This is substantially slower than in the spherical case where convergence is reached with $k = 7$ [cf. *Hirt and Kuhn*, 2012, Fig. 1]. The degree variances of the single contributions exhibit numerous intersections in spectral band of degrees ~700 to 2160, showing that much of the high-degree spectral energy is delivered by the higher-order powers. In spectral band ~1000 to 2160, powers $k = 5$ to 15 of the THFs make larger contribution than the low-integer powers 1 to 4. This behaviour is very different to the spherical case, where in spectral band of 0 to 2160 each integer power of the THF makes a contribution smaller than the previous one [cf. *Hirt and Kuhn*, 2012, Fig. 1], with the first intersection observed only around degree ~3000 [cf. *Balmino et al.*, 2012, Fig. 7].

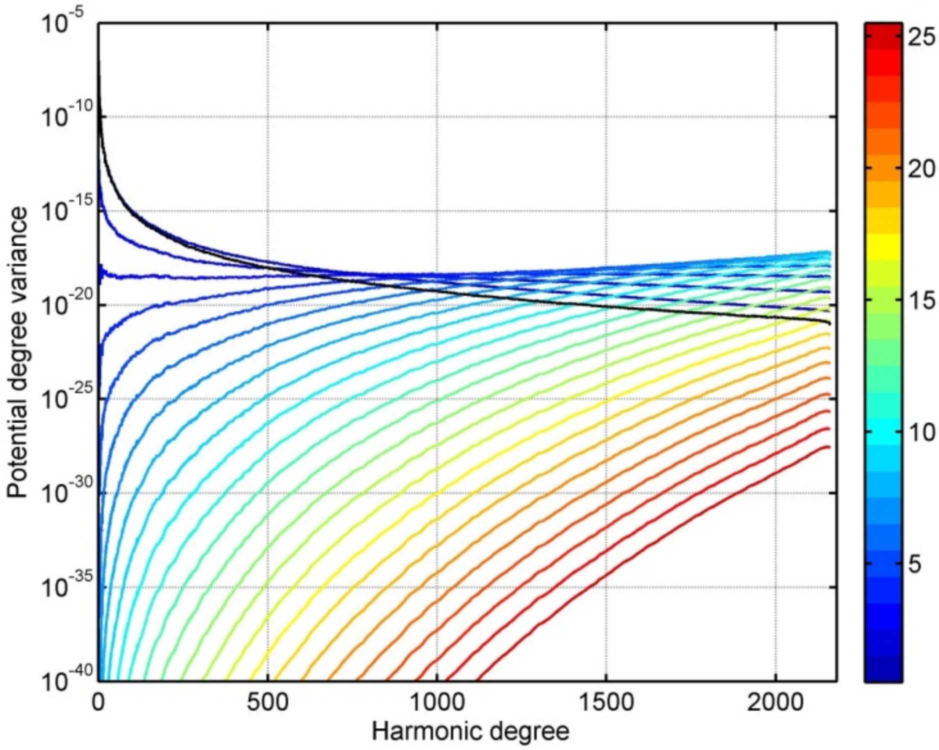

Figure 1. EI-method: Potential contributions of the first 25 integer powers of the topography. Blue: contribution of 1st power, red: contribution of 25th power. Black line: total contribution. Shown are dimensionless potential degree variances of the differences (l_Σ minus l_e).

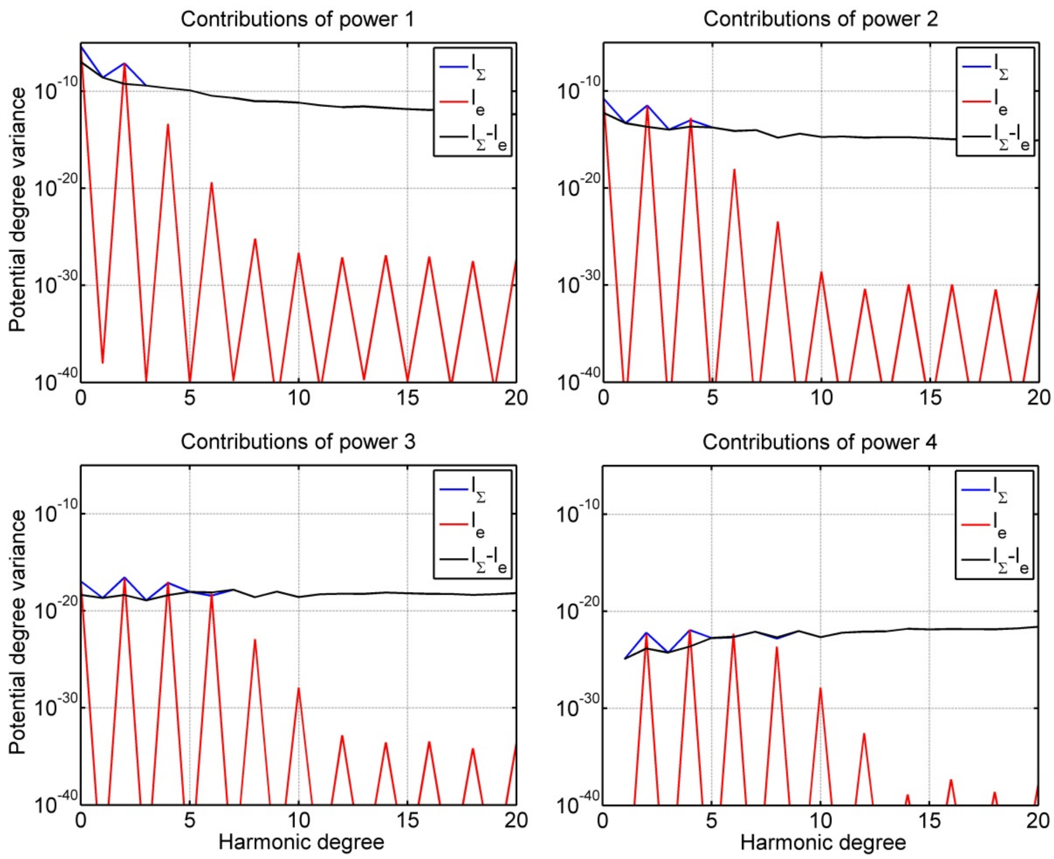

Figure 2. EI-method: Potential contributions of the first three integer powers of the topography. Shown are dimensionless potential degree variances of l_Σ, l_e and (l_Σ minus l_e).

Fig. 1 also shows that over most parts of the spectrum there are always single contributions $\bar{V}_{nm}^{R\,(k)}$ that have higher spectral energy than the total contribution $\bar{V}_{nm}^{R}$, and this effect becomes more pronounced the shorter the spatial scales. At degree 2160, the spectral power of the first 16 integer contributions is larger than that of the total contribution. Hence, addition of successive contributions has some 'cancellation effect' on the total contribution. Notwithstanding this observation, with $k = 22$ the EI-method requires a large number of integer power contributions to converge, and this is owing to the fact that the THFs are much larger than in the spherical case.

For the first four integer powers ($k = 1$ to $k = 4$) we analysed the potential contribution made by the two THFs l_{Σ}/R and l_e/R used as input in the EI-method [Eq. (15)]. As expected, the l_e/R-contributions – those of the masses between the ellipsoid and sphere – are of very long-wavelength character (Fig. 2). Akin to the potential coefficients of a normal gravity field implied by a reference level ellipsoid (e.g., GRS80), the spectral power of l_e/R is restricted to the even low-degree zonal harmonics [e.g., *Moritz*, 2000, p 130], and negligible for harmonic degrees of ~12 and larger (Fig. 2).

A detailed inspection of the l_{Σ}/R-, l_e/R-, and (l_{Σ}/R minus l_e/R)-contributions reveals that at even low-degree harmonic degrees the l_{Σ}/R-contribution is always larger than that of the difference (l_{Σ}/R minus l_e/R), hence l_e/R reduces the energy of l_{Σ}/R (note the reduction of 'spike-like effects in l_{Σ}/R in Fig. 2). Relative to the total contribution shown in Fig. 1, the spectral energy of the l_e/R–contribution is at least 10 orders of magnitudes smaller for $k \geq 4$, so can be safely neglected for all higher integer powers.

3.3 Method 2: Harmonic combination (HC) method

The convergence behaviour of method 2 (HC-method) was investigated by evaluating Eq. (29) for all indices $k = 1$ to $k = 10$ separately. The inner summations (over *j*) were evaluated to $j_{max} = 30$ which ensures convergence of these terms [cf. *Claessens* 2006, p 140, *Claessens and Featherstone* 2005, Fig. 2]. Fig. 3 shows the single contributions made by the first 10 integer powers of the THF d_{Σ}/r_e. In contrast to the EI-method, sufficient convergence is already reached for $k = 7$, which is comparable to the topographic potential contributions in spherical approximation [*Hirt and Kuhn*, 2012, Fig. 1]. In a relative sense, the behaviour of the contributions shown in Fig. 3 is comparable to the spherical case, and there are no intersections in the spectral band of degrees 0 to 2160. Due to this faster convergence, the HC-method is computationally more efficient than the EI-method.

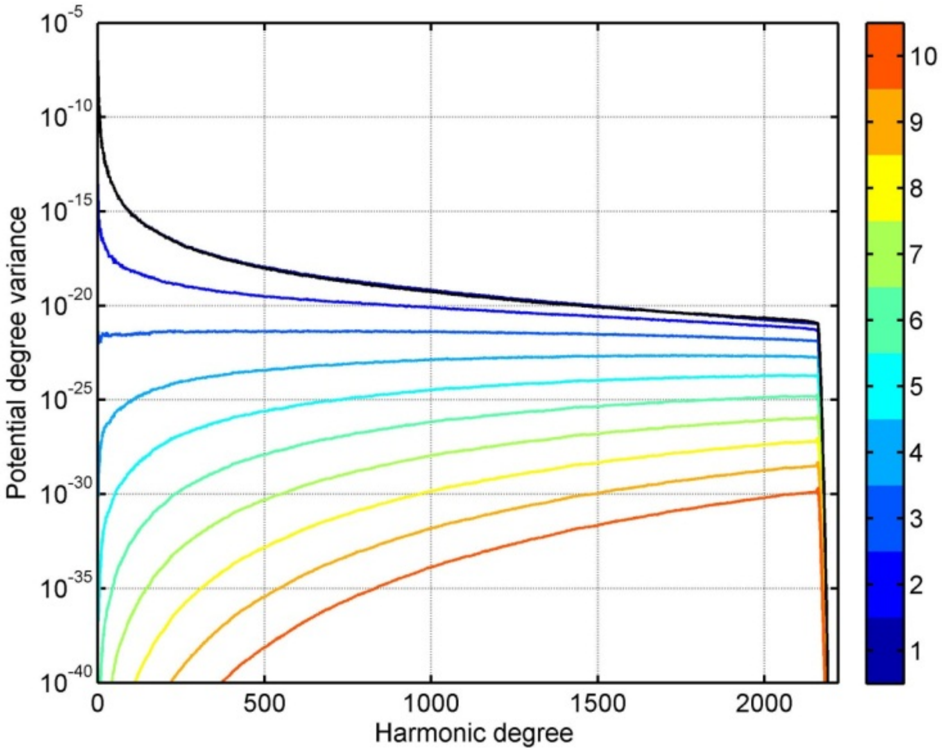

Figure 3. HC-method: Potential contributions of the first 10 integer powers of the topography. Blue: contribution of 1^{st} power, red: contribution of 10^{th} power. Shown are dimensionless potential degree variances in spectral band of degrees 0 to 2220.

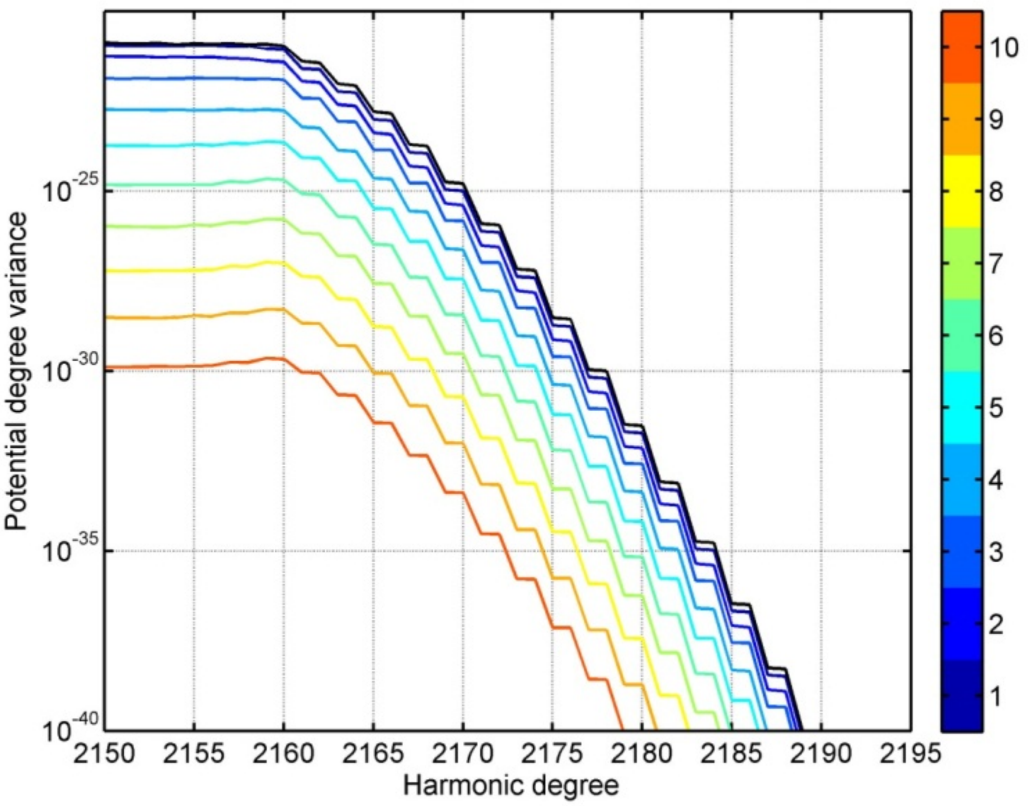

Figure 4. HC-method: As Fig. 3, but focus on spectral band of degrees 2140 to 2220.

The most important observation is made around harmonic degree 2160 where all contributions experience a drop in spectral energy. Fig. 4 provides a detail plot of all contributions in spectral band 2150 to 2195, showing that the terms $\bar{V}_{nm}^{R\,(k)}$ beyond degree 2160 make some notable contribution to about 2175, while diminishing around degree 2190. This reflects an important attribute of the HC-method. Each coefficient $\bar{V}_{nm}^{R\,(k)}$ depends on a group of SHCs $\bar{d}_{n+2i,m}^{(k)}$ within a spectral bracket of $2 \times j_{max}$ (60 in the present case) to either side of spherical harmonic degree *n*, resulting in additional SHCs of up to degree 2220 in the present case. However, because of the convergence of the summation over j in Eq. (29), the coefficients $\bar{V}_{nm}^{R\,(k)}$ become negligible beyond harmonic degree ~2180.

The observed behaviour is a key characteristic of ellipsoidal potential modelling [*Claessens*, 2006] and also seen in high-degree geopotential models such as EGM2008 [*Pavlis et al.*, 2012] that are based on ellipsoidal approximation. EGM2008 was developed in ellipsoidal harmonics to degree and order 2160 and transformed to spherical harmonics using the transformation described in *Jekeli* [1988]. In case of EGM2008, Jekeli's transformation gives rise to additional SHCs in the spectral band of degrees 2161 to 2190 as discussed in detail by *Holmes and Pavlis* [2007]. In direct analogy to EGM2008, consideration of these additional SHCs is crucially important to accurately represent the ETP, as will be demonstrated in Sect. 3.5.

3.4 Comparisons in the spectral domain

Fig. 5a compares degree variances of the (total contributions from the) EI- and HC-methods with each other, with those from (conventional) topographic potential modelling in spherical approximation [Eq. (30)], and with degree variances from the EGM2008 global gravity model. For reasons of consistency, the latter were computed from the SHCs of EGM2008, not from ellipsoidal harmonic coefficients which are also available.

The degree variances from the two ellipsoidal methods (EI and HC) are in close agreement over most of the spectrum. The spectrum of the topographic potential in spherical approximation has seemingly more power as the degree increases, with differences of about one order of magnitude at n = 2160. These differences are as expected, given different reference surfaces (surface of sphere vs. surface of ellipsoid) were used in the creation of the SHCs in spherical and ellipsoidal approximation. The reference sphere radius in spherical approximation was set equal to the semi-major axis a (the customary value), which places the topography further from the Earth's origin compared to the ellipsoidal solution, resulting in more power at higher degrees.

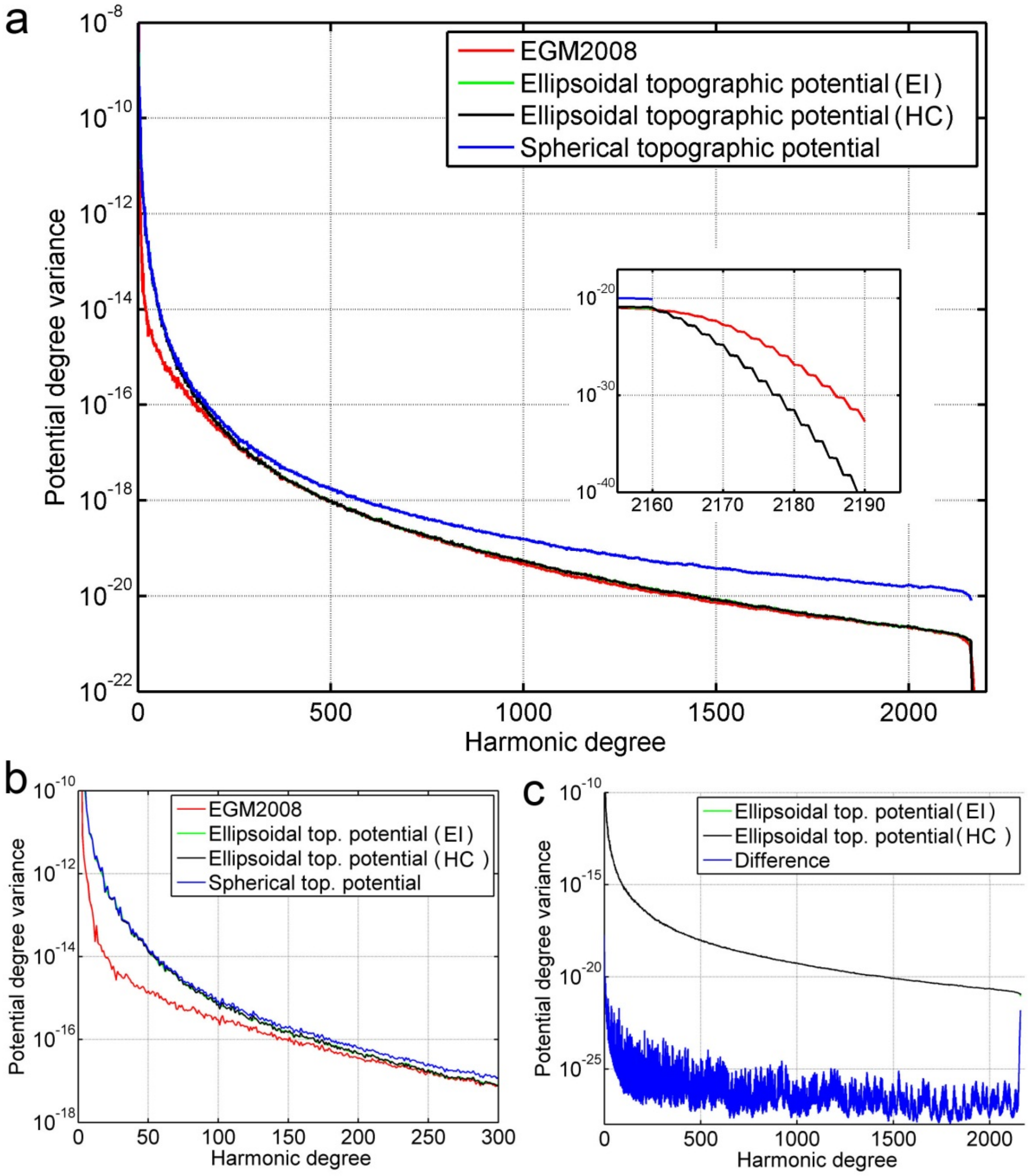

Figure 5. Comparison among the methods in the spectral domain, (a) potential degree variances of the topographic potential in spherical and ellipsoidal approximation (methods EI and HC), and of EGM2008, all in spectral band 0 to 2220 and 2150 to 2200 (close-up), (b) as before, but in spectral band 0 to 300, (c) ETP degree variances of the EI and HC-methods, and their differences in spectral band 0 to 2220.

Fig. 5b shows that the signals from the two ETP methods are commensurate with EGM2008 from harmonic degree of ~250 and higher, while the topographic potential has significantly higher power at lower harmonic degrees. This well-known behaviour is caused by isostatic compensation masses at medium and long wavelengths, which are not modelled by the (uncompensated) RET2012 topography and derived potential coefficients, but a constituent of Earth's observed gravity field, see also *Rummel et al.* [1988], *Watts* [2001], *Wieczorek* [2007], *Hirt et al.* [2012a].

Fig. 5a (inside panel) provides a detail view on the spectra of the four potential models in spectral band 2140 to 2220, exemplifying the similar characteristics of EGM2008 and the ETP from the HC-method (Sect. 3.3). Both models provide additional SHCs beyond degree 2160, which rapidly loose spectral power and reach the level of 10^{-32} (this is 10 orders of magnitude smaller than the signal) near degree 2190 for EGM2008 and near degree 2180 for the ETP.

Fig. 5c compares the degree variances of the two ETP methods, and those of their coefficient differences. The degree variances of the coefficient differences (i.e., the difference spectrum) are found to be 5 to 7 order of magnitudes smaller than the signal of the topographic potential itself. This indicates a reasonable agreement among the methods over most of the spectrum. Importantly, the spectra of the HC and EI-methods increasingly deviate from each other at high spatial degrees, as is indicated by the difference spectrum. At degree 2160, the difference spectrum is less than one order of magnitude below the signal curve, which points at a significant discrepancy among the two methods very close to the maximum degree.

3.5 Comparisons in the space domain

In order to further investigate the discrepancies among the two methods, radial derivatives of the topographic potential (also known as gravity disturbances, short: gravity) were calculated at the surface of the GRS80 ellipsoid (HC and EI methods), and at the surface of the sphere with radius R (from the topographic potential model in spherical approximation). From Fig. 6a, ellipsoidal topographic gravity from the HC-method and gravity in spherical approximation are in close agreement, with the differences (RMS 1 mGal, maximum difference 4.7 mGal) likely reflecting the effect of different mass arrangement in the two approximations. Differences in gravity from the two methods exhibit large latitude-dependent discrepancies that increase towards the poles (Fig. 6b) to magnitudes as large as ~150 mGal. These discrepancies are caused by the lack of coefficients beyond degree and order 2160 in the EI-method, as exemplified in the next paragraph. We note that the ETP from the HC-method was evaluated in our tests to degree 2190, and not to degree 2160 (e.g. Fig. 6a).

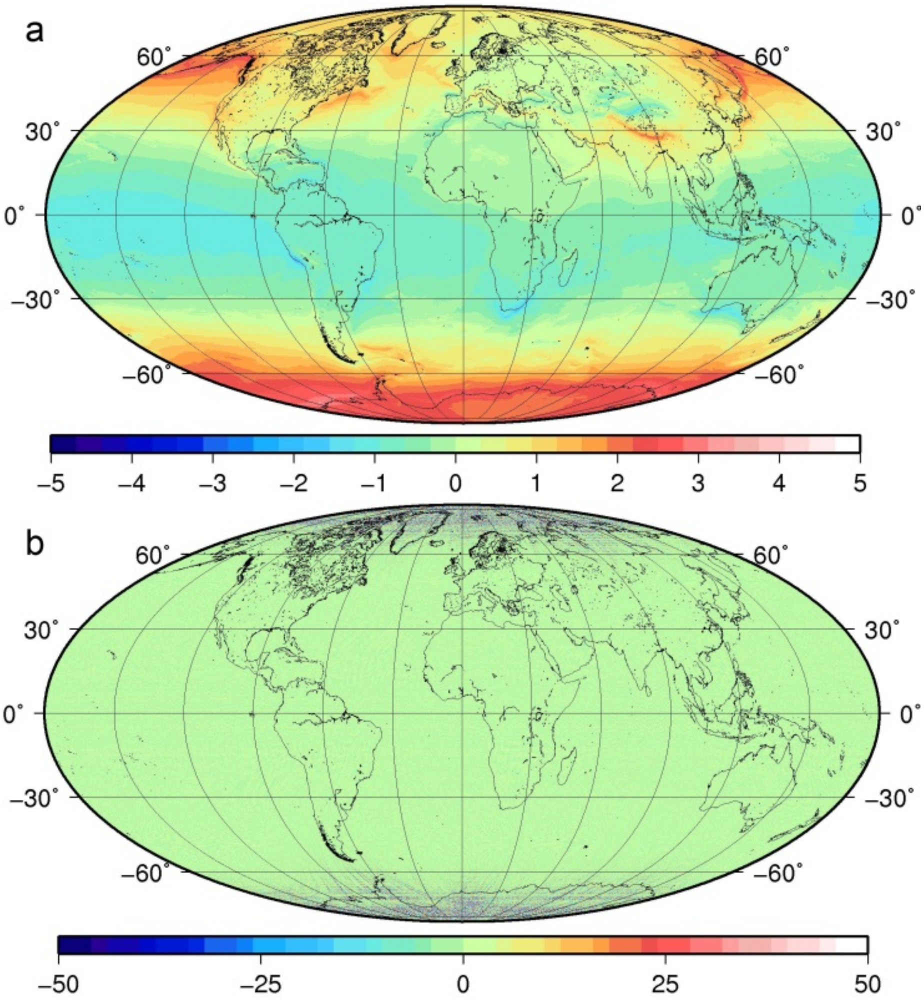

Figure 6. Comparison among the methods in the spatial domain, (a) Ellipsoidal effect: differences among gravity disturbances from HC-method in ellipsoidal approximation (band 0 to 2190) and in spherical approximation (band 0 to 2160), min/max/mean/rms = -2.9/4.7/0.6/1.2 mGal, (b) Differences among gravity disturbances from the HC- method (band 0 to 2190) and the EI-method (band 0 to 2160), min/max/mean/rms = -180/193/0/17 mGal.

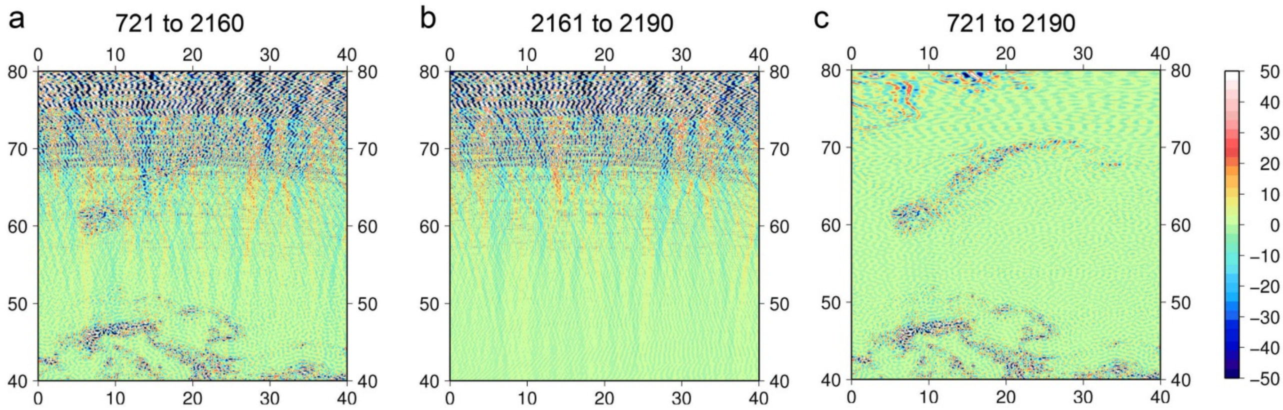

Figure 7. Gravity disturbances from the transformation method over Europe in spectral band 721 to 2160 (a), band 2161 to 2190 (b) and band 721 to 2190 (c), units in mGal.

Fig. 7 shows the importance of taking into account the SHCs beyond degree 2160 for the accurate evaluation of ETP at high degrees. Restricting the evaluation to degree 2160 produces latitude-dependent patterns in high latitudes, which increase towards the poles and reach ~100 mGal amplitudes (Fig. 7a). Similar effects were reported by *Holmes and Pavlis* [2007] for a predecessor model of EGM2008 if truncated to degree 2160. Evaluation of the SHCs beyond harmonic degree 2160 produces almost identical patterns, however, with opposite sign (Fig. 7b), which is why evaluation to degree 2190 is free of any latitude-dependent patterns Fig. 7c).

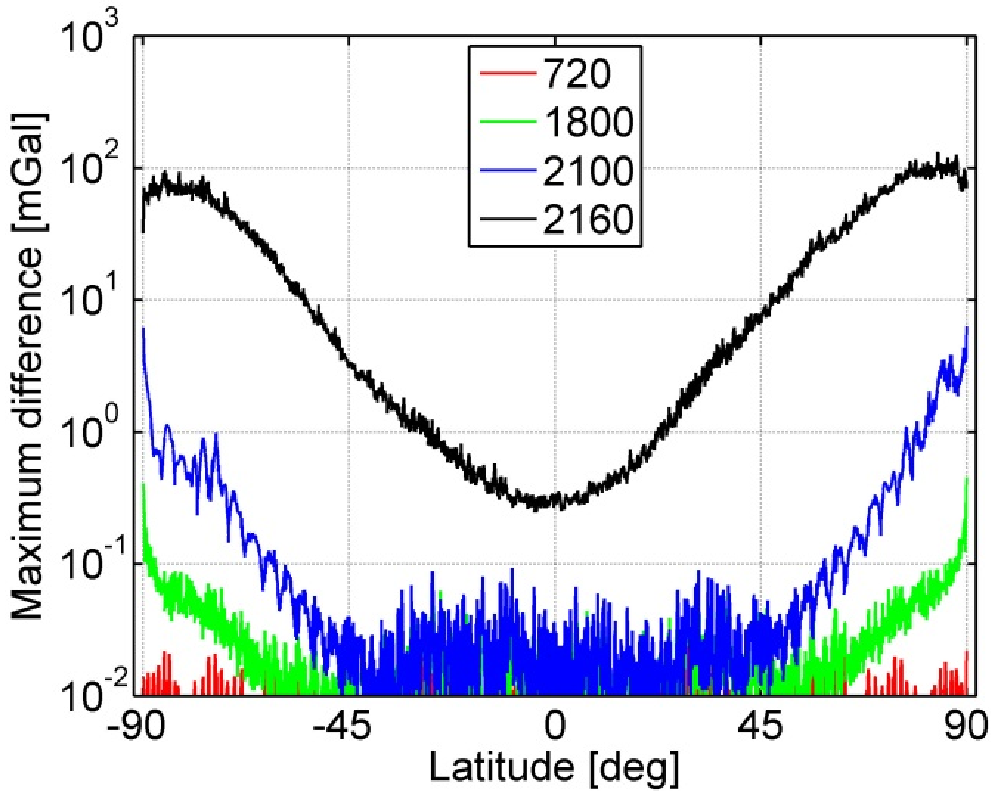

Figure 8. Maximum differences between gravity disturbances from the EI- and HC-methods along parallels for four different spectral bands (0 to 720, 0 to 1800, 0 to 2100 and 0 to 2160), units in mGal.

These comparisons provide evidence that (i) the EI and HC-methods are not rigorously compatible, and – from Fig. 6 and 7 – (ii) the latitude-dependent errors are unambiguously attributable to the EI-method. We finally attempted to narrow the discrepancies among the HC and EI-methods, by evaluating gravity disturbances from both methods in spectral bands of harmonic degrees 0 to 720, 0 to 1800, 0 to 2100 and 0 to 2160, and analysing their differences along latitude bands (similar *to Holmes and Pavlis* [2007]). Fig. 8 shows the maximum difference as a function of the latitude, and spectral bands. The agreement among gravity from both approaches is better than 0.1 mGal (expanded to degree 720), and better than 0.5 mGal (to degree 1800) anywhere on Earth (cf. Fig. 8), which is satisfactory. However, the maximum discrepancies increase to ~5 mGal (when evaluating to degree 2100) and deteriorate to ~150 mGal (degree 2160). Together with Fig. 6, this shows that the ‘problems’ with the EI-method chiefly reside in the high degrees and high latitudes, while the HC-method is free of those effects (see Fig. 6a and Fig. 7).

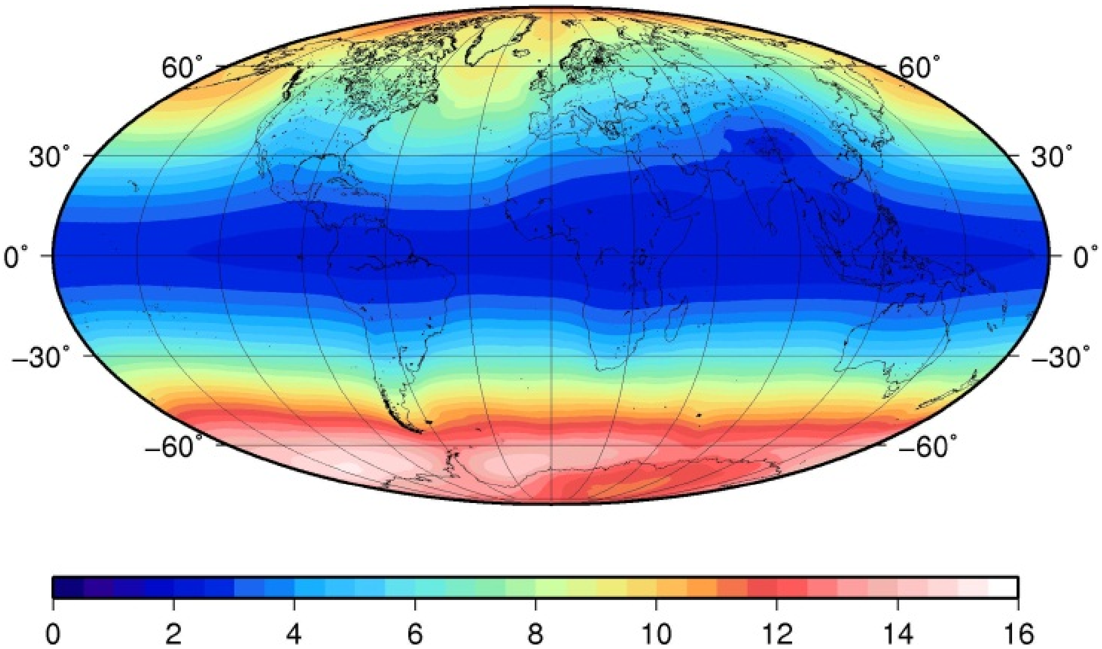

Figure 9. Ellipsoidal effect: differences among height anomalies from HC-method in ellipsoidal approximation (band 0 to 2190) and in spherical approximation (band 0 to 2160), units in m.

The differences in terms of height anomalies between the topographic potential in spherical approximation and the ellipsoidal topographic potential (using the HC-method) are shown in Fig. 9. These differences reach a magnitude of ~15 m, and are predominantly of a long-wavelength nature.

4 Application examples

We applied the HC-method (Sect 2.4) along with the RET2012 topography model (Sect. 3.1) for computation of the first degree-2190 EGM2008 Bouguer gravity map in fully-ellipsoidal approximation. We computed gravity disturbances from (i) EGM2008 and (ii) RET2012/HC in full resolution, i.e., from degree 2 to 2190 at the Earth’s surface in terms of 5 arc-min resolution grids. This was accomplished by calculating gravity disturbances and their first five radial derivatives from both models at a reference height of 4000 m above the GRS80 reference ellipsoid, and continuation of gravity disturbances from the reference height to the Earth’s surface using Taylor expansions as described in *Hirt* [2012] for EGM2008 and *Hirt and Kuhn* [2012] for the topographic potential.

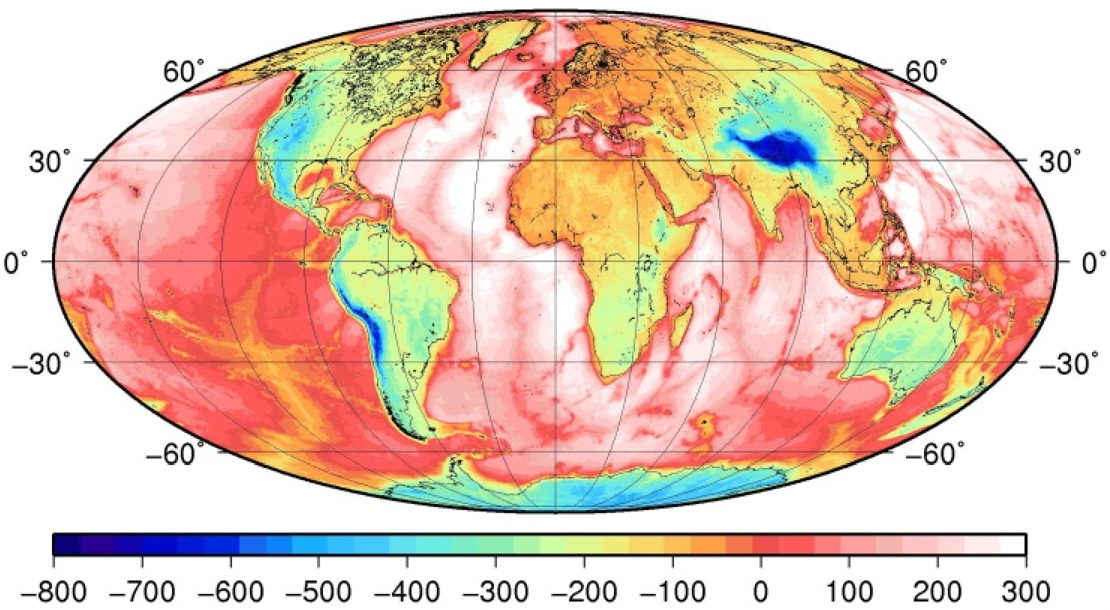

Figure 10. EGM2008 Bouguer gravity disturbances at the Earth's surface in fully-ellipsoidal approximation in spectral band 0 to 2190, topographic gravity disturbances from the HC-method, min/max/mean/rms = -964/455/-34/201 mGal.

The Earth's surface was represented by the Earth2012 surface model (http://geodesy.curtin.edu.au/research/models/Earth2012/, file Earth2012.topo_air.SHCto2160.dat). EGM2008 Bouguer gravity disturbances, obtained as difference between EGM2008 and RET2012-implied gravity effects in ellipsoidal approximation, are shown in Fig. 10. The map conceptually improves on the previously published map by *Balmino et al.* [2012], which is based on a mixture of approximation levels (topography-implied gravity effects in spherical approximation with only low-degree ellipsoidal corrections, combined with EGM2008 in full ellipsoidal approximation). From Fig. 6a, the ellipsoidal effect (i.e., differences among spherical and ellipsoidal approximation) on the topography-implied gravity is at the mGal-level, so comparatively small, but non-negligible for accurate applications.

As a second application example, we computed degree correlation coefficients among EGM2008, and the RET2012 topographic potential model in ellipsoidal (using the HC-approach) and spherical approximation (Fig. 11). The correlation among EGM2008 and the topographic potential in spherical approximation increases at low and medium degrees, reaches a maximum of about +0.85 around degree 500 before decreasing to +0.6 at degree 2000. However, a more realistic picture of the EGM2008 quality is obtained from the ellipsoidal topographic potential, with correlation coefficients found to be as large as +0.92 around degree 1000, and +0.87 at degree 2000. To our knowledge, this high correlation between geopotential and topographic potential coefficients has not been observed before. It is obvious that topographic potential SHCs in spherical approximation considerably underestimate the correlation, indicating poorer model quality at shorter spatial scales, which makes them of little use for evaluation of high-degree geopotential models such as EGM2008 which are developed in ellipsoidal approximation.

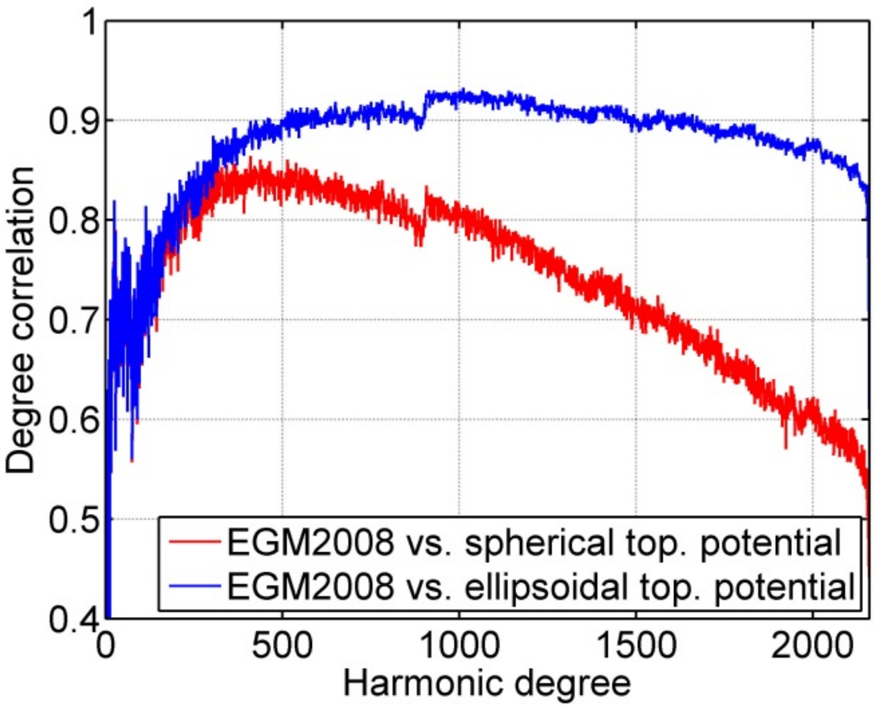

Figure 11. Degree correlation coefficients among SHCs of EGM2008 and of the implied topographic potential in spherical and ellipsoidal approximation (HC-method).

5 Discussion, conclusions and recommendations

The effect of the spherical approximation in forward gravity modelling has been shown to be significant in both the spatial and the spectral domain, especially affecting the power of high-degree topographic potential SHCs. It is therefore most crucial for quantities with substantial power in the higher degrees, and for computation of global gravity models or any type of spectral analysis. The two methods introduced here for modelling the ellipsoidal topographic potential, though distinctly different in their approach, show good agreement across almost the entire spectrum. It can be concluded that of the two methods, the harmonic combination method is superior, because i) it provides faster convergence and hence requires less powers of the THFs, and more importantly ii) it provides additional coefficients beyond degree 2160 that are vital for accurate evaluation of the ETP.

The correlation between the ETP and EGM2008 coefficients was found to be much greater for the ellipsoidal approximation than for the spherical approximation. Not only do the degree variance spectra of the ETP and EGM2008 exhibit similar power from degree ~250 onwards, the degree correlation coefficients are also much higher than for the spherical approximation. These numerical results clearly show that the solution in ellipsoidal approximation delivers a significant improvement over the spherical approximation. We recommend that the harmonic combination method be used for spectral forward gravity modelling of any celestial object that can closely be approximated by an oblate ellipsoid of revolution.

Acknowledgements

The Australian Research Council (ARC) is acknowledged for funding through Discovery Project grant DP120102441. Christian Hirt is the recipient of an ARC Discovery Outstanding Researcher Award.

References

Bagherbandi M., and L.E. Sjöberg (2012), A synthetic Earth gravity model based on a topographic-isostatic model, *Stud. Geophys. Geod.*, 56(2012), 935-955, doi: 10.1007/s11200-011-9045-1.

Balmino, G. (1994), Gravitational potential harmonics from the shape of an homogeneous body, *Celest. Mech. Dynam. Astron.*, 60(3), 331-364.

Balmino, G., K. Lambeck, and W.M. Kaula (1973), A spherical harmonic analysis of the Earth's topography, *J. Geophys. Res.*, 78(2), 478-481.

Balmino, G., N. Vales, S. Bonvalot and A. Briais (2012), Spherical harmonic modelling to ultra-high degree of Bouguer and isostatic anomalies, *J. Geod.*, 86(7), 499-520, doi: 10.1007/s00190-011-0533-4.

Claessens, S.J. (2003), A synthetic Earth model: analysis, implementation, validation and application, *DUP Science*, Delft, The Netherlands.

Claessens, S.J. (2005), New relations among associated Legendre functions and spherical harmonics, *J. Geod.*, 79(6-7), 398-406, doi: 10.1007/s00190-005-0483-9.

Claessens, S.J. (2006), *Solutions to Ellipsoidal Boundary Value Problems for Gravity Field Modelling*, PhD thesis, Curtin University of Technology, Department of Spatial Sciences, Perth, Australia.

Claessens, S.J., and W.E. Featherstone (2005), Computation of geopotential coefficients from gravity anomalies on the ellipsoid, in *A Window on the Future of Geodesy*, IAG Symposia vol. 128, ed F Sanso, 459-464.

Driscoll J.R., and D.M. Healy (1994), Computing Fourier transforms and convolutions on the 2-sphere, *Adv. in Appl. Math.*, 15, 202-250.

Eshagh, M. (2009), Comparison of two approaches for considering laterally varying density in topographic effect on satellite gravity gradiometric data. *Act. Geoph.*, 58(4), 661-686, doi: 10.2478/s11600-009-0057-y.

Fukushima, T. (2013), Recursive computation of oblate spheroidal harmonics of the second kind and their first-, second-, and third-order derivatives, *J. Geod.*, 87(4), 303-309, doi: 10.1007/s00190-012-0599-7.

Göttl, F., and R. Rummel (2009), A geodetic view on isostatic models. *Pure Appl. Geophys.* 166(8-9), 1247-1260, doi:10.1007/s00024-004-0489-x.

Grafarend, E.W., and J. Engels (1992), A global representation of ellipsoidal heights – geoidal undulations or topographic heights – in terms of orthonormal functions. *Manusc. Geod.*, 17, 52-58.

Grafarend, E.W., and J. Engels (1993), The gravitational field of topographic-isostatic masses and the hypothesis of mass condensation, *Surv. Geophys.*, 14(4-5), 495-524, doi: 10.1007/BF00690574.

Grombein, T., K. Seitz, and B. Heck (2013), Topographic-isostatic reduction of GOCE gravity gradients. In *Proc. of the XXV IUGG General Assembly* Melbourne, Australia 2011, IAG Symposia, vol. 139 (accepted for publication).

Haagmans, R. (2000), A synthetic Earth model for use in geodesy, *J. Geod.*, 74(7-8), 503-511, doi: 10.1007/s001900000112.

Heck, B., and K. Seitz (2007), A comparison of the tesseroid, prism and point-mass approaches for mass reductions in gravity field modelling, *J. Geod.*, 81(2), 121–136, doi: 10.1007/s00190-006-0094-0.

Heck, B., and F. Wild (2005), Topographic-isostatic reductions in satellite gravity gradiometry based on a generalized condensation model, in *A Window on the Future of Geodesy*, IAG Symposia vol. 128, ed F Sanso, 294-299.

Holmes S.A., and N.K. Pavlis (2007), Some aspects of harmonic analysis of data gridded on the ellipsoid, in *Gravity Field of the Earth*, Proceed. 1st International Symposium of the International Gravity Field Service, Istanbul, Turkey, Harita Dergisi, 151-156.

Hirt, C. (2012), Efficient and accurate high-degree spherical harmonic synthesis of gravity field functionals at the Earth's surface using the gradient approach, *J. Geod.*, 86(9), 729-744, doi: 10.1007/s00190-012-0550-y.

Hirt, C. (2013), RTM gravity forward-modeling using topography/bathymetry data to improve high-degree global geopotential models in the coastal zone, *Marine Geod.*, 36(2):1–20, doi:10.1080/01490419.2013.779334.

Hirt, C., and M. Kuhn (2012), Evaluation of high-degree series expansions of the topographic potential to higher-order powers, *J. Geophys. Res.*, 117, B12407, doi:10.1029/2012JB009492.

Hirt, C., S.J. Claessens, M. Kuhn, and W.E. Featherstone (2012a), Kilometer-resolution gravity field of Mars: MGM2011. Planetary and Space Science 67(1), 147-154, doi: 0.1016/j.pss.2012.02.006.

Hirt, C., M. Kuhn, W.E. Featherstone, and F. Göttl (2012b), Topographic/isostatic evaluation of new-generation GOCE gravity field models, *J. Geophys. Res.*, 117, B05407, doi:10.1029/2011JB008878.

Jekeli, C. (1988), The exact transformation between ellipsoidal and spherical harmonic expansions, *Manusc. Geod.*, 13(2), 106-113.

Kuhn, M., and W.E. Featherstone (2003), On the optimal spatial resolution of crustal mass distributions for forward gravity modelling, in *Gravity and Geoid 2002*, Proceed. 3rd Meeting of the International Gravity and Geoid Commission, ed IN Tziavos, Ziti Editions, Thessaloniki, 189-194.

Kuhn, M., and K. Seitz (2005), Comparison of Newton's Integral in the Space and Frequency Domains, in *A Window on the Future of Geodesy*, IAG Symposia vol. 128, ed F Sanso, 386-391.

Lambeck, K. (1979), Methods and geophysical applications of satellite geodesy. *Rep. Prog. Phys.*, 42: 547-628, doi:10.1088/0034-4885/42/4/001.

Mladek, F. (2006), Hydrostatische Isostasie (in German). IAPG/FESG Report No. 24, Institut fur Astronomische und Physikalische Geodasie, Universitat Munchen, Germany.

Mohr P.J., B.N. Taylor, and D.B. Newell (2012), "The 2010 CODATA Recommended Values of the Fundamental Physical Constants" (Dated: March 27, 2012, Web Version 6.3). Available from http://physics.nist.gov/constants.

Moritz, H. (2000), Geodetic Reference System 1980. *J. Geod.*, 74, 128-140.

Novák, P. (2010), Direct modelling of the gravitational field using harmonic series, *Acta Geodyn. Geomater.*, 7(1), 35-47.

Novák, P., and E.W. Grafarend (2005), Ellipsoidal representation of the topographical potential and its vertical gradient. *J. Geod.*, 78(11-12), 691-706, doi:10.1007/s00190-005-0435-4.

Pavlis N.K., and R.H. Rapp (1990), The development of an isostatic gravitational model to degree 360 and its use in global gravity modelling. Geophys. J. Int., 100, 369-378.

Pavlis N.K., S.A. Holmes, S.C. Kenyon, and J.K. Factor (2012), The development and evaluation of the Earth Gravitational Model 2008 (EGM2008), *J. Geophys. Res.*, 117, B04406, doi:10.1029/2011JB008916.

Ramillien, G. (2002), Gravity/magnetic potential of uneven shell topography, *J. Geod.*, 76(3), 139-149, doi:10.1007/s00190-002-0193-5.

Rapp, R.H. (1982), Degree variances of the Earth's potential, topography and its isostatic compensation. *Bull. Geod.*, 56(2), 84-94, doi:10.1007/BF02525594.

Rummel, R., R.H. Rapp, H. Sünkel, and C.C. Tscherning (1988), Comparisons of global topographic/isostatic models to the Earth's observed gravity field, Report No 388, Dep. Geodetic Sci. Surv., Ohio State University, Columbus, Ohio.

Sebera J., J. Bouman, and W. Bosch (2012), On computing ellipsoidal harmonics using Jekeli's renormalization. *J. Geod.*, 86(9), 713-726, doi:10.1007/s00190-012-0549-4.

Sjöberg, L.E. (1998), The exterior Airy/Heiskanen topographic-isostatic gravity potential anomaly and the effect of analytical continuation in Stokes' formula, *J. Geod.*, 72(11), 654-662, doi:10.1007/s001900050205.

Sjöberg, L.E. (2004), The ellipsoidal corrections to the topographic geoid effects, *J. Geod.*, 77(12), 804-808, doi:10.1007/s00190-004-0377-2.

Sona, G. (1995), Numerical problems in the computation of ellipsoidal harmonics, *J. Geod.*, 70(1-2), 117-126, doi:10.1007/BF00863423.

Sun, W., and L.E. Sjöberg (2001), Convergence and optimal truncation of binomial expansions used in isostatic compensations and terrain corrections, *J. Geod.*, 74(9), 627–636, doi:10.1007/s001900000125.

Sun, W. (2002), A formula for gravimetric terrain corrections using powers of topographic height. *J. Geod.*, 76(8), 399-406, doi: 10.1007/s00190-002-0270-9.

Sünkel, H. (1986), Global topographic-isostatic models, in Mathematical and Numerical Techniques in Physical Geodesy, Lecture notes in Earth Sciences, vol. 7, Springer, ed H. Sünkel, 417-462.

Tenzer, R., Z. Hamayun, and I. Prutkin (2010), A comparison of various integration methods for solving Newton's integral in detailed forward modelling, in *Gravity, Geoid and Earth Observation*, IAG Symposia, vol. 135, 361-368, ed SP Mertikas , doi: 10.1007/978-3-642-10634-7_48.

Tenzer, R., P. Novák, P. Vajda, V. Gladkikh, and Hamayun (2012), Spectral harmonic analysis and synthesis of Earth's crust gravity field, *Comput. Geosci.*, 16: 193-207, doi:10.1007/s10596-011-9264-0

Tsoulis, D. (1999), Spherical harmonic computations with topographic/isostatic coefficients. IAPG/FESG Report No. 3, Institut fur Astronomische und Physikalische Geodasie, Universitat Munchen, Germany.

Tsoulis, D. (2001), A comparison between the Airy/Heiskanen and the Pratt/Hayford isostatic models for the computation of potential harmonic coefficients, *J. Geod.*, 74(9), 637-643, doi:10.1007/s001900000124.

Vajda P, Vaníček P, Novák P, Tenzer R, Ellmann A (2007) Secondary indirect effects in gravity anomaly data inversion or interpretation, *J. Geophys. Res.*, 112: B06411, doi: 10.1029/2006JB004470

Völgyesi, L., and G. Toth (1992), Optimal topographic-isostatic crust models for global geopotential interpretation. Periodica Polytechnica Civ. Eng., 36(2), 207-241.

Wang, Y.M., and X. Yang (2013) On the spherical and spheroidal harmonic expansion of the gravitational potential of topographic masses, *J. Geod.*, online first, doi:10.1007/s00190-013-0654-z

Watts, A.B. (2001), *Isostasy and Flexure of the Lithosphere*. Cambridge University Press, Cambridge, United Kingdom.

Wieczorek, M.A. (2007), Gravity and topography of the terrestrial planets. in *Treatise on Geophysics*, 10, 165-206, Elsevier-Pergamon, Oxford, United Kingdom.

Wieczorek, M.A., and R.J. Phillips (1998), Potential anomalies on the sphere: Applications to the thickness o the lunar crust, *J. Geophys. Res.*, 103(E1), 1715-1724, doi:10.1029/97JE03136.

Wild-Pfeiffer F., and B. Heck (2007), Comparison of the modelling of topographic and isostatic masses in the space and the frequency domain for use in satellite gravity gradiometry, in *Gravity Field of the Earth*, Proceed. 1st International Symposium of the International Gravity Field Service, Istanbul, Turkey, Harita Dergisi, 312-317.

Appendix A: Legendre weight functions

The fully normalised sinusoidal Legendre weight functions $\bar{K}_{nm}^{2i,2j}$ in Eq. (25) can be computed via various recursive schemes [*Claessens* 2005]

$$\bar{K}_{nm}^{2i,2j} = \sum_{k=-1}^{1} \bar{K}_{nm}^{2i-2k,2j-2} \bar{K}_{n+2i-2k,m}^{2k,2} \tag{A1}$$

$$\bar{K}_{nm}^{2i,2j} = \sum_{k=-1}^{1} \bar{K}_{nm}^{2k,2} \bar{K}_{n+2k,m}^{2i-2k,2j-2} \tag{A2}$$

$$\bar{K}_{nm}^{2i,2j} = \sum_{k=-1}^{1} \bar{K}_{nm}^{2i+2k,2j-2} \bar{K}_{n+2i,m}^{2k,2} \tag{A3}$$

where (A3) follows from (A1) and the relation

$$\bar{K}_{nm}^{2i,2j} = \bar{K}_{n+2i,m}^{-2i,2j} \tag{A4}$$

Equations (A1) to (A3) can all be used to compute the function $\bar{K}_{nm}^{2i,2j}$ for any pair of *i* and *j* from the initial values

$$\bar{K}_{nm}^{-2,2} = -\sqrt{\frac{(n^2-m^2)[(n+1)^2-m^2]}{(2n-3)(2n-1)^2(2n+1)}} \tag{A5}$$

$$\bar{K}_{nm}^{0,2} = \frac{2(n^2+m^2+n-1)}{(2n-1)(2n+3)} \tag{A6}$$

$$\bar{K}_{nm}^{2,2} = -\sqrt{\frac{[(n+1)^2-m^2][(n+2)^2-m^2]}{(2n+1)(2n+3)^2(2n+5)}} \tag{A7}$$

The initial values shown here only hold for the fully-normalised (4π-normalised) functions. Any other form of normalisation will not affect the recursion relations, but will result in different initial values, which can easily be derived. Details on the practical and numerical differences between the various recursive schemes can be found in *Claessens* [2005].